

Convection in Multiphase Fluid Flows Using Lattice Boltzmann Methods

L. Biferale,^{1,2} P. Perlekar,² M. Sbragaglia,¹ and F. Toschi^{2,3}

¹*Department of Physics and INFN, University of Tor Vergata, Via della Ricerca Scientifica 1, 00133 Rome, Italy*

²*Department of Physics, Eindhoven University of Technology, 5600 MB Eindhoven, The Netherlands*

³*Department of Mathematics and Computer Science, and J.M. Burgerscentrum, Eindhoven University of Technology, 5600 MB Eindhoven, The Netherlands; and CNR-IAC, Viale del Policlinico 137, 00161 Roma, Italy*

(Received 24 October 2011; published 7 March 2012)

We present high-resolution numerical simulations of convection in multiphase flows (boiling) using a novel algorithm based on a lattice Boltzmann method. We first study the thermodynamical and kinematic properties of the algorithm. Then, we perform a series of 3D numerical simulations changing the mean properties in the phase diagram and compare convection with and without phase coexistence at Rayleigh number $Ra \sim 10^7$. We show that in the presence of nucleating bubbles non-Oberbeck-Boussinesq effects develop, the mean temperature profile becomes asymmetric, and heat-transfer and heat-transfer fluctuations are enhanced, at all Ra studied. We also show that small-scale properties of velocity and temperature fields are strongly affected by the presence of the buoyant bubble leading to high non-Gaussian profiles in the bulk.

DOI: 10.1103/PhysRevLett.108.104502

PACS numbers: 47.20.Bp, 47.11.Qr, 47.27.-i, 47.55.-t

Thermal convection, the state of a fluid heated from below and cooled from above, is a ubiquitous phenomena in nature, present in many industrial and geophysical applications both at micro- and macroscales [1]. It is also challenging from theoretical points of view, raising questions on pattern formations for small temperature jumps between the bottom and top plates (i.e., moderate Rayleigh number) or on turbulent behavior where the heat transfer (i.e., Nusselt number) is dominated by bulk or boundary layer physics (or by both, see e.g., recent reviews [2]). Thermal convection is often studied in the Oberbeck-Boussinesq (OB) approximation, where a single phase—unstratified—fluid is present with constant material properties. Compressibility is also neglected except for buoyancy forces. Needless to say, in many situations some, or all, of the above assumptions break down and one speaks of non-Oberbeck-Boussinesq (NOB) convection. Deviations from OB approximation can arise in many different ways. One notable case is boiling: when the parameters' excursion inside the convective cell allows for phase coexistence [3,4]. In this Letter we study thermal convection in a 3D cell in a high turbulent regime where large bubbles (larger than the turbulent viscous scale) can nucleate in the layer close to the bottom wall with a non-negligible heat exchange between liquid and vapor. To do that, we present and apply a novel numerical scheme based on a diffuse interface lattice Boltzmann method (LBM) [5]. In such a way, we are not restricted to treat bubbles as pointlike [6] and we fully resolve the thermohydrodynamical properties of the gas and liquid phases. Besides the methodological aspects, we also address physical questions connected to the enhancement or depletion of heat flux in the presence of bubbles, statistics of mean global properties, as well as small-scale effects for both velocity and temperature fluctuations. We present two series of high-resolution numerical simulations up to 512^3

collocation points at $Ra \sim 10^7$ with and without phase coexistence, such as to be able to directly compare on the same geometrical setup the effect of boiling on convection. We also present some data obtained in 2D geometries to address the important point of heat-flux dependency on the Rayleigh number. With respect to experimental studies, numerical simulations offer the unique advantages of allowing access to all quantities without affecting the fluid dynamics and confining the fluid inside “ideal” surfaces (i.e., perfect thermal properties at the wall, perfect smoothness of the boundaries, etc.). On the other hand, a limitation consists in the difficulty to reach high Rayleigh numbers and to push the physical parameters such as density contrast, interface thickness, viscosity, and thermal diffusivity to realistic situations. The equations of motion describing a nonideal fluid in the presence of thermal fluctuations are:

$$\partial_t \rho u_i + \partial_j (\rho u_i u_j) = -\partial_i P + \partial_j [\mu (\partial_i u_j + \partial_j u_i)] + g \rho \hat{z} \quad (1)$$

where $\mu = \rho \nu$ is the molecular viscosity, g is the gravity, ρ is the local fluid density, and $P(\rho, T) = P_0(\rho, T) + P_{\text{NI}}(\rho)$ is the nonideal pressure. Pressure is fixed by the equation of state and it is made of the ideal part $P_0(\rho, T) = \rho T$ and the nonideal part which in our LBM system reads: $P_{\text{NI}}(\rho) = G \exp(-2/\rho)$ (see below). The equation for the internal energy, $U = c_v T + \int d\rho P_{\text{NI}}/\rho^2$ is given by one of the two following equivalent expressions:

$$\begin{aligned} c_p \rho D_t T - \beta T D_t P &= \kappa \partial_{jj} T \\ c_v \rho D_t T + P_0 \partial_j u_j &= \kappa \partial_{jj} T \end{aligned} \quad (2)$$

where κ is the thermal conductivity, D_t stands for the material derivative, c_v is the specific heat at constant volume, and c_p and $\beta = -(\partial_T \rho)/\rho$ are the specific heat and compressibility at constant pressure, respectively. The

above equations tend to the usual OB system when the fluid is single phase, incompressible, and both μ, κ are constant [7]. In Table I we report the characteristic values for all relevant parameters for two typical runs, with and without boiling.

Because of bubble nucleation and evaporation, a key role is played by the $D_t P$ term in (2). Take, for example, a convective cell of size L with imposed temperature, T_d , at the bottom wall and T_u at the top wall. Then, the heat balance across a horizontal layer at distance z from the bottom wall is:

$$\partial_t \overline{\rho U}|_z + \partial_z \overline{\rho U u_z} - \kappa \partial_z \overline{T}|_z = -\overline{P \partial_j u_j}|_z \quad (3)$$

where with $\overline{(\cdot \cdot \cdot)}|_z$ we intend a spatial average at fixed z . In a stationary situation, we can define a z -dependent dimensional Nusselt number $\text{Nu}(z) = \overline{\rho U u_z} - \kappa \partial_z \overline{T}|_z$ which satisfies an integral constraint

$$\text{Nu}(z) - \text{Nu}(0) = -\int_0^z dz' \overline{P \partial_j u_j}|_{z'}. \quad (4)$$

With the above definition, the Nusselt number is not anymore constant throughout the cell, we may exchange heat by nucleating and evaporating bubbles or by simple compressible effects inside each phase.

Algorithm.—The numerical algorithm used is based on discrete kinetic models [5]. The starting point is a standard coupled mesoscopic dynamics described by [5,8]:

$$f_l(\mathbf{x} + \mathbf{c}_l, t + 1) - f_l(\mathbf{x}, t) = -\frac{1}{\tau_\nu} (f_l - f_l^{(\text{eq})})(\mathbf{x}, t), \quad (5)$$

$$g_l(\mathbf{x} + \mathbf{c}_l, t + 1) - g_l(\mathbf{x}, t) = -\frac{1}{\tau_\kappa} (g_l - g_l^{(\text{eq})})(\mathbf{x}, t), \quad (6)$$

where $f_l(\mathbf{u}, t)$, $g_l(\mathbf{x}, t)$ stand for the probability density functions to find at (\mathbf{x}, t) a particle whose kinetic velocity belongs to a discrete and limited set \mathbf{c}_l (with $l = 1, 19$ in the $D3Q19$ LBM adopted here [5]). Density, momentum, and temperature are defined as coarse-grained (in velocity space) fields of the distribution functions

TABLE I. Typical values for boiling and nonboiling runs in 3D. $\Delta \tilde{T}$, $\Delta \tilde{c}_p$, $\Delta \tilde{\beta}$ are values of temperature, liquid heat capacity, and the liquid compressibility jump between the two walls (all normalized with their values at the center of the cell, z_c). $\chi_{l,g} = \kappa / (c_p(z_c) \rho_{l,g}(z_c))$ is the thermal diffusivity of liquid (l) and gas (g). ν is the kinematic viscosity. Rayleigh (Ra) and Prandtl (Pr) numbers are evaluated at z_c and in the liquid phase. $\text{Ra} = \frac{g \beta(z_c) L^4 (\Delta T / L - \gamma_{ad}(z_c))}{k / (\rho(z_c) c_p(z_c)) \nu}$ and $\text{Pr} = \frac{\nu}{\chi^{(l)}(z_c)}$ where $L = 512$ is the cell height (in grid units) and $\gamma_{ad} = \beta T g / c_p$ is the adiabatic gradient. The Jacob number quantifying the ratio between the sensible heat and the latent heat [6] is $\text{Ja} \sim 3$.

	$\Delta \tilde{T}$	$\Delta \tilde{c}_p$	χ_g	χ_l	ν	Ra	$\Delta \tilde{\beta}$	Pr
Boiling	0.226	1.2	0.008	0.0018	0.0165	3×10^7	1.6	9
No boil	0.230	0.2	...	0.0018	0.0165	2×10^7	0.1	9

$$\rho = \sum_l f_l \quad \rho \mathbf{u} = \sum_l \mathbf{c}_l f_l \quad T = \sum_l g_l. \quad (7)$$

The local kinetic equilibria $f_l^{(\text{eq})}(\mathbf{u}', \rho)$ and $g_l^{(\text{eq})}(\mathbf{u}, F, T)$ are expanded in a polynomial basis [9] such that a Chapman-Enskog expansion [8] leads to the equations for density, momentum, and temperature (1) and (2): the streaming step on the left-hand side of (5) reproduces the inertial terms in the hydrodynamical equations, whereas dissipation and thermal diffusion are connected to the relaxation (towards equilibrium) properties in the right-hand side, with ν and κ related to the relaxation times τ_ν, τ_κ [5]. Nonideal thermodynamics is obtained by a well controlled procedure shifting the velocity in the equilibrium distribution, $\mathbf{u}' = \mathbf{u} + \tau_\nu \mathbf{F} / \rho$, with a forcing term mimicking the effect of an internal pseudopotential [8,9]. We adopt the standard form:

$$F = -\mathcal{G} \sum_{l=1}^N w(|\mathbf{c}_l|^2) \mathbf{c}_l \psi[\rho(\mathbf{x})] \psi[\rho(\mathbf{x} + \mathbf{c}_l)] \quad (8)$$

where \mathcal{G} is the strength of the nonideal interactions. The weights $w(|\mathbf{c}_l|^2)$ are used to enforce isotropy up to the 4th order in the velocity tensors [10]. The pseudopotential, $\psi[\rho]$, encompasses the macroscopic effects of both long-range attraction and short-range repulsion. Although various choices have been presented for the choice of $\psi[\rho]$ [11,12], here it is crucial to set it to $\psi[\rho] = \exp(-1/\rho)$, in such a way to reproduce the thermodynamic consistency on the lattice [13] (see Fig. 1). The ideal part of the pressure, $P_0 = \rho T$, is obtained via a coupling between f_l and g_l populations by plugging the dynamical temperature

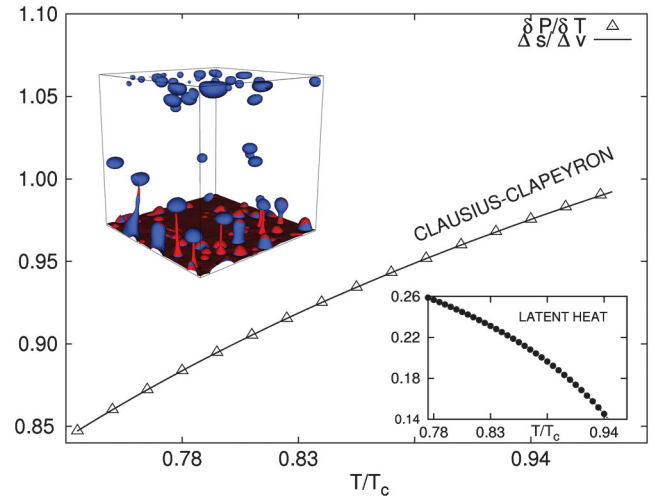


FIG. 1 (color). Mechanical-thermal coupling in our LBM (Clausius-Clapeyron relation): $\partial P / \partial T = \Delta s / \Delta v$ at varying T / T_c . P is the equilibrium pressure at coexistence temperature T , $v = 1/\rho$ is the specific volume, T_c is the critical temperature, and $s(T, \rho)$ is the specific entropy. Bottom inset: Latent heat, $\lambda = T \Delta s$ vs T . Top inset: Bubbles are in blue. Regions with high temperature are in red. The system has no-slip velocity at the bottom and top walls and it is periodic on the horizontal directions.

T in the equilibrium distribution of (6) (see [14]). In the limit of vanishing interaction, this is equivalent to imposing a second order momentum of $f_l^{(eq)}$ equal to $\sum_i f_l^{(eq)} c_i^i c_l^j = \rho T \delta_{ij} + \rho u_i u_j$. Finally, in order to get the divergence term, $P_0 \partial_j u_j$, in (2), we added a counterterm to the evolution of g_l populations in (6), as proposed in [15]. As a result, neglecting extra viscous contributions at the interface [16], we ended with a LBM for the Navier-Stokes (NS) Eqs. (1) and (2) with a nonideal pressure tensor and a consistent definition of latent heat (see Fig. 1).

Single point quantities.—In Fig. 2 we show a scatter plot of $T(\mathbf{x}, t)$ vs $\rho(\mathbf{x}, t)$ for a boiling cell. Superposing with the equilibrium curves in the T - ρ phase space, we see that most of the volume is at *thermodynamical equilibrium*. The presence of bubbles is clearly detected by the spots concentrating along the vapor branch. It is interesting to notice that the corresponding bubble temperature is always larger than the mean temperature in the cell, indicating that bubbles are transferring temperature upwards very efficiently. Moreover, the temperature profile across the cell, $\overline{T(z)}$, becomes slightly asymmetric in the presence of bubbles, a phenomenon also observed in other liquidlike NOB systems [17]. Breaking of the top-down symmetry should not be a surprise. In particular, β is not constant across the cell (i.e., density and temperature fluctuations are not strictly proportional as in the OB system) and c_p decreases going from bottom to top. Both effects may have an impact on the averaged profiles as discussed and observed also in [17]. Here, the temperature mismatch between the values at the center and the mean temperature is 1% (inset of top panel in Fig. 2). Notice also that $\overline{T(z)}$ agrees with the expected profile given by the adiabatic gradient, due to the presence of a small stratification. In the bulk, the heat flux (4) is dominated by the convective term $\overline{\rho U u_z}$. In the bottom panel of Fig. 2 we compare the Nusselt number for the boiling and nonboiling cell at similar Rayleigh numbers. Two effects show up. First, heat flux is enhanced. Second, fluctuations around its mean profile are larger in the presence of bubbles. We interpret this as a clear signature of the importance of the bubble dynamics in transporting heat between the two walls. This is the combined effect of temperature entrainment inside bubbles leveraged with the upward buoyancy of a bubble. Because bubbles are rare in our system, this also implies an increase in heat-flux fluctuations, as can be seen in the inset of the bottom panel in Fig. 2 where we show the probability density function (PDF) of the heat flux measured only in the bulk cell. Clearly, the right tails are enhanced, due to bubble buoyancy. The residual small oscillation in the bulk-heat-flux profile for the boiling case would probably vanish with a longer integration time and/or by removing the bubble layer forming at the top plate. In Fig. 3 we show the trend in Nusselt vs Rayleigh numbers obtained by combining both simulations in the 3D and 2D setup (the latter to increase the Rayleigh number). As one

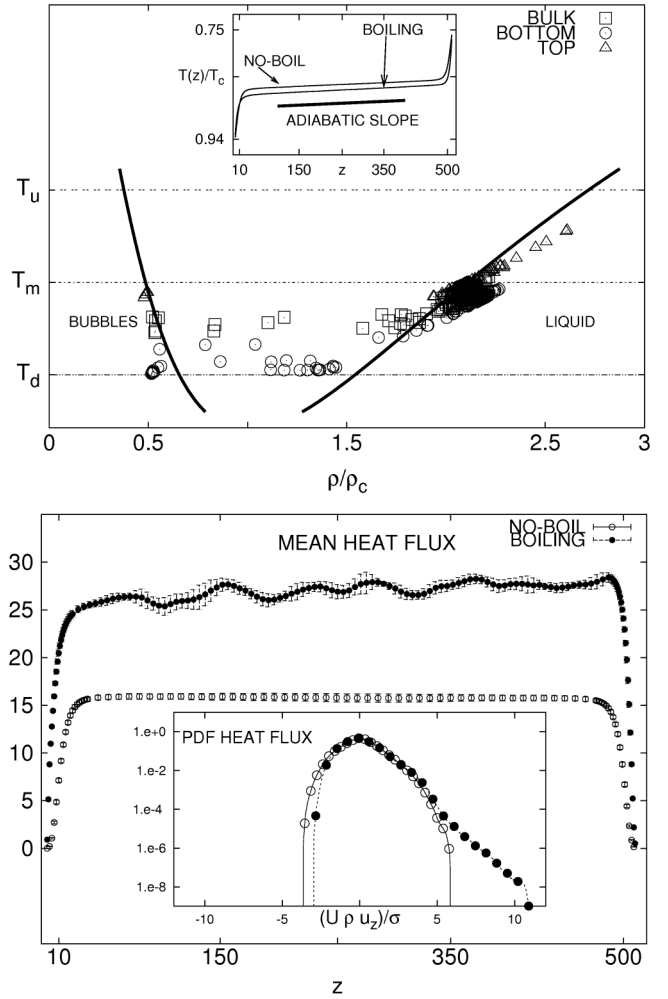


FIG. 2. Top panel: Phase space T - ρ equilibrium curves (solid lines) superposed with a scatter plot of temperature and density values at boiling (both made dimensionless using the critical values, T_c and ρ_c). Notice the presence of bubbles with different temperatures inside the volume. Different symbols correspond to measurements taken in the top, bottom, or bulk region. The horizontal dashed lines correspond to top, T_u , bottom, T_d , and mean, T_m , temperatures. Inset: Mean temperature profile, $\overline{T(z)}/T_c$ vs z (in lattice units) for boiling and nonboiling conditions. The straight line corresponds to the adiabatic slope. Bottom panel: Bulk contribution to the heat flux normalized to its diffusive value, $\overline{\rho U u_z}/[\kappa(T_d - T_u)/L]$, (Nusselt) for boiling and nonboiling cases at comparable Rayleigh numbers. Inset: PDF of $\rho U u_z$ normalized to have mean area and mean variance for both boiling and nonboiling cases.

can see, the trend respects the well known $Nu \propto Ra^{1/3}$ for all cases, with a consistent systematic enhancement of heat transfer for boiling systems.

Small-scale properties.—Buoyant bubbles bring information from the physics of the bottom boundary layer in the bulk of the system. We then expect also in the bulk an increase of small-scale velocity and temperature fluctuations. In Fig. 4 we show the structure functions for vertical velocity and temperature:

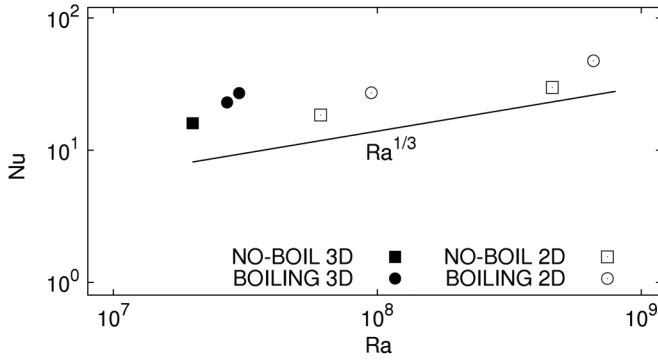


FIG. 3. Nu vs Ra for 3D and 2D convection with and without boiling. Notice the systematic enhancement of heat flux for boiling systems. Statistical error bars are of the order of the point size.

$$\begin{aligned} S_{u_z}^{(p)}(r) &= \langle [u_z(\mathbf{x} + \mathbf{r}) - u_z(\mathbf{x}) \cdot \hat{\mathbf{r}}]^p \rangle_{\text{bulk}} \\ S_T^{(p)}(r) &= \langle [T(\mathbf{x} + \mathbf{r}) - T(\mathbf{x}) \cdot \hat{\mathbf{r}}]^p \rangle_{\text{bulk}} \end{aligned} \quad (9)$$

where the average is restricted on points \mathbf{x} in the bulk of the cell and the increment \mathbf{r} is always taken in horizontal directions. In the two panels of Fig. 4 we show the results for both quantities for $p = 2$. For both fields we have a viscous range very well resolved, where the structure functions are $\propto r^2$. Therefore, the presence of large bubbles does not destroy the differentiability at small scales, another signature that the numerical setup is under control. Second, a boiling system has an enhanced signal at small scales, meaning that energy dissipation is globally increased. Third, for the boiling case we start to see an inertial range with scaling $\propto r^{2/3}$, similar to the Kologorov 1941 concept of turbulence. In the inset of both panels we measure the flatness (or kurtosis) of each field $K_{u_z, T}(r) = S_{u_z, T}^{(4)}(r) / [S_{u_z, T}^{(2)}(r)]^2$ at different scales, e.g., is a way to quantify how much the PDF is close or different from a Gaussian. Intermittency, as measured by the deviation of the flatness from its Gaussian value, $K = 3$, becomes more and more important at decreasing the scale, in agreement with the general observation that bubbles induce an increase of fluctuations in the system. For temperature (top panel Fig. 4) the inertial range behavior is much more singular than the case for velocity, due to the enhancement of temperature jumps between inside and outside bubbles. In contrast to the case for velocity, where large scale PDF is indistinguishable from a Gaussian ($K_{u_z} \sim 3$ for $r \sim L$), here temperature is more sensitive to the presence of bubbles also at large scale.

In conclusion, we have proposed a novel LBM to attack multiphase flows with a full consistent definition of heat exchange in the system (latent heat). We have applied this scheme to study convection under a boiling condition and we have studied the effects of nucleating large bubbles at the bottom boundary layer on both single-point observable (temperature profile and heat-flux) and two-point

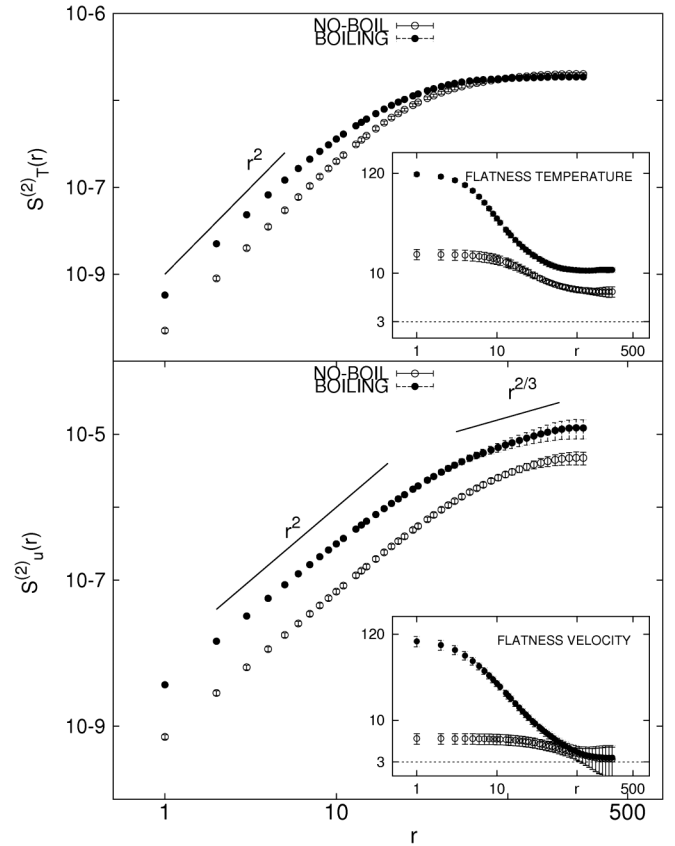


FIG. 4. Second order structure function for velocity (bottom) and temperature (top) vs r (in lattice units) for boiling and nonboiling systems. Inset: values of flatness (same symbols).

correlation functions (structure functions). The latter, allowed us to assess also the importance of bubbles on small-scale velocity and temperature fluctuations, indicating an enhancement of the deviations from Gaussian statistics with respect to the nonboiling case.

We acknowledge useful discussion with R. Verzicco. We acknowledge computational support from CINECA (IT), CASPUR (IT), and SARA (NL) and from the DEISA Extreme Computing Initiative (FP6 Projects No. RI-031513 and No. FP7 RI-222919). M.S. acknowledges support from DROEMU-FP7 IDEAS Contract No. 279004.

- [1] P. Cardin and P. Olson, *Phys. Earth Planet. Inter.* **82**, 235 (1994); G.A. Glatzmaier and P.H. Roberts, *Nature (London)* **377**, 203 (1995).
- [2] E. Bodenschatz, W. Pesch, and G. Ahlers, *Annu. Rev. Fluid Mech.* **32**, 709 (2000); G. Ahlers, S. Grossmann and D. Lohse, *Rev. Mod. Phys.* **81**, 503 (2009).
- [3] J.-Q. Zhong, D. Funfschilling and G. Ahlers, *Phys. Rev. Lett.* **102**, 124501 (2009).
- [4] V.K. Dhir, *Annu. Rev. Fluid Mech.* **30**, 365 (1998).
- [5] S. Succi, *The Lattice Boltzmann Equation* (Oxford Science, New York, 2001).

-
- [6] P. Oresta *et al.*, *Phys. Rev. E* **80**, 026304 (2009).
[7] A. Spiegel and G. Veronis, *Astrophys. J.* **131**, 442 (1960).
[8] B. Shi and Z. Guo, *Phys. Rev. E* **79**, 016701 (2009); Z. Guo, C. Zheng, and B. Shi, *Phys. Rev. E* **65**, 046308 (2002).
[9] X. Shan and H. Chen, *Phys. Rev. E* **47**, 1815 (1993); Sbragaglia *et al.*, *J. Fluid Mech.* **628**, 299 (2009).
[10] M. Sbragaglia *et al.*, *Phys. Rev. E* **75**, 026702 (2007).
[11] P. Yuan and L. Schaefer, *Phys. Fluids* **18**, 042101 (2006).
[12] A.L. Kupershtokh, D.A. Medvedev, and D.I. Karpov, *Comput. Math. Appl.* **58**, 965 (2009).
[13] M. Sbragaglia and X. Shan, *Phys. Rev. E* **84**, 036703 (2011).
[14] J. Zhang and F. Tian, *Europhys. Lett.* **81**, 66005 (2008).
[15] N.I. Prasianakis and I. V. Karlin, *Phys. Rev. E* **76**, 016702 (2007).
[16] P.J. Dellar, *Phys. Rev. E* **65**, 036309 (2002).
[17] Ahlers *et al.*, *Phys. Rev. E* **77**, 046302 (2008); *J. Fluid Mech.* **569**, 409 (2006).